Available online at www.sciencedirect.com

ScienceDirect

Geochimica et Cosmochimica Acta 269 (2020) 413–428

Geochimica et Cosmochimica Acta

www.elsevier.com/locate/gca

Fluid transport and reaction processes within a serpentinite mud volcano: South Chamorro Seamount

C. Geoffrey Wheat [a,*], Jeffrey S. Seewald [b], Ken Takai [c]

[a] College of Fisheries and Ocean Sciences, University of Alaska Fairbanks, PO Box 475, Moss Landing, CA 95039, USA
[b] Woods Hole Oceanographic Institution, MS# 04, Woods Hole, MA 02543, USA
[c] Subground Animalcule Retrieval (SUGAR) Project, Frontier Research System for Extremophiles, Japan Agency for Marine-Earth Science and Technology, 2-15 Natsushima-cho, Yokosuka 237-0061, Japan

Received 1 February 2019; accepted in revised form 27 October 2019; available online 4 November 2019

Abstract

Natural fluids with a pH (25 °C) up to 12.3 were collected from a sub-seafloor borehole observatory (Ocean Drilling Program (ODP) Hole 1200C) on South Chamorro Seamount, a serpentinite mud volcano in the Mariana forearc. We used systematic differences in the chemical compositions of pore waters from drilling operations during ODP Leg 195 and borehole fluids collected subsequently from Hole 1200C to define two endmember solutions, one of which was a sulfate-rich fluid with a methane concentration of 50 mM that ascends from the subduction channel and the other was a low-sulfate fluid. The sequence of sample collection and fluid compositions constrain subsurface hydrologic conditions. Deep-sourced, sulfate- and methane-rich, sterile fluids from the subduction channel can reach the seafloor unchanged within the central conduit, whereas other fluid pathways likely intersect the pelagic sediment that underlies the serpentinite mud volcano, providing potentially suitable conditions and inoculum for microbial anaerobic oxidation of methane (AOM). These AOM-affected, low-sulfate fluids also make it to the seafloor where they discharge. The source of the sulfate- and methane-rich fluid in the subduction channel is attributed to abiotic methane production fueled by hydrogen production from serpentinization and carbonate dissolution. This methane production includes a mechanism to raise the pH above values from serpentinization alone. Results from South Chamorro Seamount represent an end member along a transect defined by the distance from the trench. Results from this site are applied to other serpentinite mud volcanoes along this transect to speculate on likely chemical conditions within shallower and cooler portions of the subduction channel.

Keywords: Serpentinization; Mud volcano; Subduction; Mariana forearc; Dissolved gases; Anaerobic methane oxidation

1. INTRODUCTION

The Mariana forearc is the home of tens of active serpentinite mud volcanoes, which are the largest mud volcanoes on Earth, some spanning 50 km in diameter and kilometers high (Fryer and Fryer, 1987). Currently serpentinite mud volcanoes are known to form only in the Mariana forearc; however, the geologic record indicates that serpentinite volcanism occurred throughout Earth's history as far back as 3.8 billion years ago (Pons et al., 2011). These serpentinite mud volcanoes form at the intersection of faults in a non-accretionary forearc prism. Such faults form from backarc crustal extension resulting in along strike extension in the forearc (Latouche et al., 1981), plate roll-back resulting in across–strike extension (Fryer and Fryer, 1987), and subduction of seamounts that cause vertical extension (Fryer et al., 2018). This faulting

* Corresponding author.
E-mail addresses: wheat@mbari.org (C.G. Wheat), jseewald@whoi.edu (J.S. Seewald), kent@jamstec.go.jp (K. Takai).

https://doi.org/10.1016/j.gca.2019.10.037
0016-7037/

permits fluids, muds, clasts, and rocks to be transported from the subduction channel to the seafloor, forming serpentinite mud volcanoes. Because these active serpentinite mud volcanoes are located at different distances to the trench that correspond to different depths, temperatures, and pressures within the subduction channel, they offer an opportunity to study physical, thermal, chemical, and microbial processes within a subduction channel without the expense of deep drilling. Thermal conditions of subduction, for example, are critical to elucidating stresses, strain, and plate movement within a subduction system (e.g., Saffer and Tobin, 2011).

Characterizing conditions and processes during the early stages of subduction has been addressed using a variety of methodologies. In the Mariana forearc such characterizations include seismic (Oakley et al., 2007, 2008) and bathymetric surveys (Fryer, 1992), seafloor drilling and coring (Fryer et al., 1990; Salisbury et al., 2002; Fryer et al., 2018; Fryer et al., 1999, Mottl et al., 2004; Hulme et al., 2010), and dredging studies (Bloomer and Hawkins, 1987). Each of these approaches presents a "snap-shot" of current conditions. While such studies provide significant results, they lack a temporal component necessary to elucidate dynamic processes associated with serpentinite mud volcanism and plate subduction.

In 2001, the Ocean Drilling Program (ODP) drilled and cased Hole 1200C in the summit knoll of South Chamorro Seamount, an active serpentinite mud volcano in the Mariana forearc (Salisbury et al., 2002). This borehole tapped a hydrologic zone that discharged fluids that were highly altered relative to seawater composition (Wheat et al., 2008). These fluids were alkaline with a pH (25 °C) up to 12.5 and contained dissolved methane and sulfate (Mottl et al., 2003). In addition to providing a platform from which to characterize temporal processes and conduct in situ experiments, Hole 1200C also provided a means to collect pristine crustal fluids directly using gas-tight samplers as they discharged. This aspect of the borehole design was critical for obtaining reliable dissolved gas data, which can be used to constrain chemical conditions and the extent of serpentinization within the subduction channel, subsurface microbial metabolic potential, and mass balances of water and materials.

We present chemical data from fluids that discharged from Hole 1200C in 2009 to provide an assessment of dissolved gas concentrations within a serpentinite mud volcano, sub-crustal fluid pathways, and reactions within the subduction channel and to constrain microbial provinces within and below this serpentinite mud volcano. We also discuss processes within the subduction channel closer to the trench where conditions are cooler and shallower, suggesting a continuum of processes during the initial stage of plate subduction.

2. GEOLOGIC SETTING AND SAMPLE COLLECTION

South Chamorro Seamount is a 20 km-wide serpentine mud volcano with a summit region that is ~4 km in diameter at ~3150 m water depth (Fig. 1). A 200 m-wide knoll that is 200 m high with a 2 km wide base exists at the summit. It is located at the edge of a headwall scar which, based on bathymetric data, revealed a 70 km-long debris flow originating from the summit (Fryer et al., 2000). The knoll is also part of the current conduit for deep-sourced fluids from the underlying and subducting Pacific plate. These fluids have a pH (25 °C) as high as 12.5 and are sulfate- and methane-rich (Mottl et al., 2003, 2004; Hulme et al., 2010), with sulfate originating from the subducting Pacific Plate, based analysis of pore waters from Conical Seamount with a similar fluid composition (Alt and Shanks, 2006; Komar and Mottl, 2005). Such fluids support subsurface chemosynthetic microbial communities of archaea and bacteria (Takai et al., 2005: Curtis et al., 2013; Kawagucci et al., 2018) whose primary production support megafaunal communities that include mussels, gastropods, tubeworms, and galatheid crabs (Fryer and Mottl, 1997; Kyuno et al., 2009; Chen et al., 2016).

Six boreholes were drilled into the summit knoll of South Chamorro Seamount during ODP Leg 195 to study the subsurface transport of serpentinite material in an active serpentinite mud volcano (Salisbury et al., 2002). Hole 1200C was drilled to 266 meters below the seafloor (mbsf) prior to the deployment of a screened/cased borehole and an oceanic borehole observatory, commonly called a CORK (Circulation Obviation Retrofit Kit, Davis et al., 1992; Salisbury et al., 2002). The final configuration placed the base of the CORK at 202.8 mbsf with a screened section from 148.8 mbsf to 202.3 mbsf (Salisbury et al., 2002) (Fig. 2A). The screened section provides a pathway for pore waters to enter the borehole where they can be sampled, avoiding sampling artifacts associated with the recovery of serpentinite muds and the extraction of pore waters and dissolved gases.

In 2003 the seal to Hole 1200C was removed. Thirty-seven days later fluids were collected that discharged through the borehole from a positively pressured formation (~170 kPa; Vinas, 2013) that was bisected by the screened portion of the casing (Wheat et al., 2008). Prior to collection, fluids were diluted with bottom seawater (~60% seawater) that entered the borehole through latch holes within the near-seafloor borehole structure. This mixture of seawater and formation fluid ascended the remaining 69 cm of the borehole structure at a rate of 2 cm sec^{-1}, during which brucite and carbonate minerals precipitated, precluding the sampling of pristine fluids (Wheat et al., 2008). The borehole was subsequently sealed.

In January 2009 we returned to Hole 1200C with the remotely operated vehicle *HyperDolphin* (HPD Dives 941–947) during a JAMSTEC-funded cruise (NT09-01) to sample pristine fluids (Kawagucci et al., 2018). During the first dive (HPD941) borehole fluids that were trapped within the casing prior to our arrival (herein termed stagnant fluids) were collected from the fluid sampling port on the side of the original-styled CORK (Davis et al., 1992). Fluids were collected using a sampling reservoir designed to minimize inadvertent entrainment of ambient bottom seawater. One end of a tube was attached to the CORK sampling port with an aeroquip quick disconnect while the other end was attached to a clear polycarbonate

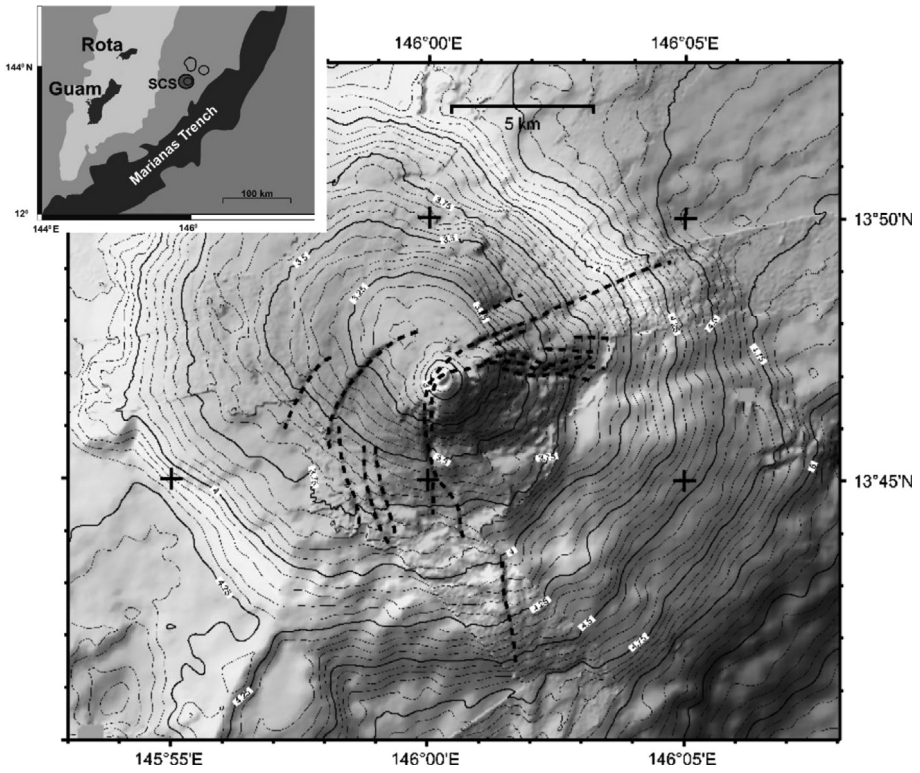

Fig. 1. South Chamorro Seamount (SCS) is located east of the northern portion of Guam and west of the Mariana Trench. This serpentinite mud volcano rises from a water depth of ~4250 m to 2930 m. Faults are indicated by dashed lines on the bathymetric map (contour lines every 50 m) consistent with the more recent slope failures to the southeast. The headwall has been overprinted by "more recent" serpentinite eruptions that formed a knoll on the summit. This knoll has a generally flat top that is ~200 m wide and ~200 m shallower than much of the summit region. This knoll was drilled during ODP Leg 195 during which the casing and CORK in Hole 1200C were deployed (Salisbury et al., 2002).

reservoir fitted with a rubber flap, which served as a check valve. After flushing the polycarbonate reservoir with borehole fluid several sampling devices were inserted through the rubber flap to collect pristine borehole fluids (Kawagucci et al., 2018). Sampling devices included isobaric gas-tight samplers (Seewald et al., 2002), WHATS II (Saegusa et al., 2006; Miyazaki et al., 2017) and a large volume bag sampler.

The CORK seal was subsequently removed, allowing the formation to discharge freely. Two days latter during dive HPD945, two days after the seal was removed, we inserted a standard 3-in. schedule 120 polyvinyl chloride (PVC) tube with o-ring seals, which was designed to seal the latch holes at the seal sleeve (International Ocean Discovery Program (IODP) part number OJ6038-2), resulting in the delivery of pristine formation fluids to the top of the borehole where they could be sampled. Assuming the borehole discharged at ~1 cm sec^{-1} (40% of the estimated rate from 2003 that included 60% dilution by seawater; Wheat et al., 2008) almost two borehole volumes of fluid were expelled before we sampled discharging fluids by placing the intakes of the various samplers at least 10 cm into the open borehole. Discharging fluids were sampled again during Dive HPD947. Fluids from both dives (HPD945 and HPD947) had identical compositions (Kawagucci et al., 2018). The borehole remained open and was revisited in May–June 2009 during which discharging fluids were sampled with the WHATS and large bag sampler during dives HPD1007, 1009, and 1010 (JAMSTEC cruise NT09-07) that occurred 126, 128, and 129 days after the seal was removed, respectively, (Kawagucci et al., 2018). The borehole was left open and observations of venting formation fluids were documented in 2012 during additional *HyperDolphin* dives (Kawagucci et al., 2018).

3. ANALYTICAL METHODS

Three types of samples are discussed; pore waters that were extracted during drilling operations (Salisbury et al., 2002; Mottl et al., 2003), borehole fluids recovered in 2003 (Wheat et al., 2008), and better quality borehole fluids that were recovered during a series of *HyperDolphin* dives in 2009 (Kawagucci et al., 2018). For completeness we describe methods that were used to analyze fluids from 2009 in Supplemental Materials.

4. RESULTS

Two distinct fluid compositions were identified during the drilling of ODP Site 1200 in 2001 (Salisbury et al., 2002; Mottl et al., 2003). The deeper fluid had seawater-like sulfate concentrations (28 mmol/kg), an alkalinity of

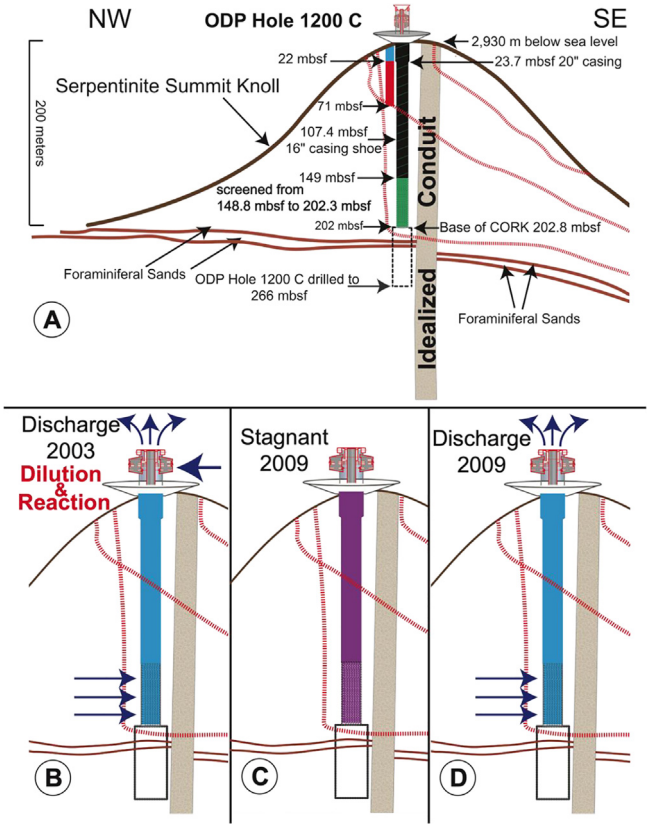

Fig. 2. Diagram of relevant chemical compositions of pore waters and fluids in the context of the cased borehole and geologic setting at ODP Hole 1200C on South Chamorro Seamount (Salisbury et al., 2002). (A) Details of the CORK installation and pore water results are shown as a function of depth. The blue region represents the low-sulfate, AOM-affected, pore waters and the red region represents the deep-sourced, sulfate-rich pore waters. The black region represents the borehole casing and the green region represents the screened portion of the casing. (Red lines denote faults and brown lines represent foraminiferal sands. (B) Fluids that discharged in 2003 were low in sulfate and entered the borehole through the screened portion (Wheat et al., 2008). (C) From 2003 to 2009 the borehole was sealed. Initial sampling in 2009 revealed a borehole fluid that was intermediate in composition between the low-sulfate and sulfate-rich fluids (Kawagucci et al., 2018). (D) Fluids that discharged in 2009 were low in sulfate (Kawagucci et al., 2018). (Modified from Wheat et al., 2008).

62 mmol/kg, no measurable sulfide, and a pH (25 °C) of 12.5 (Table 1). In contrast a shallow fluid, which was observed only in the upper 17 m of Hole 1200E, had a nearly depleted sulfate concentration (<1 mmol/kg), an alkalinity of 127 mmol/kg, a sulfide concentration of ~ 19.5 mmol/kg, and a pH (25 °C) of 12.2.

Two distinct fluids were collected from the borehole at Hole 1200C in 2009 (Table 1). The "stagnant" fluid that was collected (HPD941) prior to removing the seal was characterized by a sulfate concentration of 12.1 mmol/kg, an alkalinity of 93.0 mmol/kg, a sulfide concentration of 7.5 mmol/kg, and a pH (25 °C) of 12.28. The methane concentration of this fluid was 33.4 mmol/L. Dissolved H_2 concentrations were stable at 56 μmol/L. In contrast, the second fluid collected from the top of the borehole after it was flushed was a "low-sulfate discharging fluid" with a methane concentration of 23 mmol/L, based on data from the isobaric gas-tight samplers. Discharging fluids had a maximum dissolved H_2 concentration of 142 μmol/L (HPD945 and HPD 947). The measured dissolved H_2 concentrations systematically decreased over the 1- to 2-h it took to process samples. Stable values were attained when the concentrations reached ~8 μmol/L. Because the fluids remained on *HyperDolphin* for several hours following collection and resided in the shipboard laboratory for a few hours prior to processing, the measured concentration of H_2 likely underestimates the *in situ* abundance. Similar decreases in the measured concentrations of dissolved H_2 during sample processing were observed in samples from low temperature diffuse fluids from 9°50′N on the East Pacific Rise and were attributed to microbial consumption (McNichol et al., 2016).

Within error, both the stagnant and discharging fluids collected in 2009 are characterized by chloride concentrations of 507 mmol/kg, a value that is lower than the bottom seawater concentration of 538 mmol/kg (Table 1). Measured Na and K concentrations were also similar in the stagnant and discharging fluids (614 and 15.8 mmol/kg, respectively), but were substantially enriched relative to bottom seawater. Dissolved Mg and Ca concentrations were ≤ 0.2 mmol/kg, reflecting the low solubility of Mg- and Ca-bearing hydroxide and carbonate minerals in highly alkaline, carbonate-rich fluids (e.g., Mottl et al., 2004). Note there are differences in the composition of pore

Table 1
Fluid composition of samples from ODP Site 1200, South Chamorro Seamount. Pore water data were compiled from Salisbury et al. (2002), Mottl et al. (2003), and Komar and Mottl (2005) where the sulfate-rich pore water is based on an average of asymptotic values. The 2003 data are from Wheat et al. (2008) and were subjected to dilution with bottom seawater and precipitation of brucite and carbonate minerals before collection. The 2009 fluids are an average from Kawagucci et al. (2018). The sulfate-rich, deep-sourced fluid is an average of or calculated (in parenthesis) values from this work and data from the ODP Site 1200.

Name in Paper	Bottom Water	Low-Sulfate Pore Water 1200E 4H-1	Sulfate-rich Pore Water ODP Site 1200	2003	Stagnant Fluid HPD941	Low-Sulfate Discharging Fluid	Sulfate-rich Deep Fluid Compiled
	2009			2003	2009	2009	**(Calculated)**
pH (25 °C)	7.9	12.21	12.5	12.2	12.28	12.1	12.5
Sulfate[1]	28.1	0.64	28	2.3	12.1	0.8	28
Sulfide[1]	0	19.5	<0.25	19	7.5	24.8	<0.25
Alkalinity[1]	2.64	127	62	104	93	120	62
$\delta^{13}CCO_2$ (PDB)	–	–	−15	–	1.7	2.6	–
Methane (mM)	<0.001	–	2	–	33.4	23	**(50)**
$\delta^{13}CCH_4$ (PDB)	–	–	−14.5	–	−26.4	−37.4	**(−18.4)**
δDCH_4	–	–	–	–	−113.3	−104.8	–
Hydrogen (mM)	<0.002	–	–	–	0.056	<0.1	**(200)**
Formate (uM)	–	–	–	–	9.80	5.9	–
Acetate (uM)	–	–	–	–	33.6	38	–
$\delta^{34}S$ SO_4 (CDT)	20.5	–	about 20	–	–	–	about 20
Cl[1]	538	512	510	509	504	507	510
Na[1]	463	620	610	614	611	614	613
Na/Cl (molar)	0.86	1.21	1.2	1.21	1.21	1.21	1.21
K[1]	10.2	19.0	19	17.6	15.5	15.8	15.6
Mg[1]	52.5	0	<0.01	0	0.13	0.2	0.1
Ca[1]	10.3	0	0.3	0	0.2	0.1	0.2
Li[2]	26.2	1.3	0.4	5.4	3.7	3.7	3.7
Rb[2]	1.31	9.7	11	7	7.6	7.7	7.7
Cs[3]	2.3	62		130	102	102	102
Sr[2]	88.3	3.6	10	0	9	10	10
Ba[2]	0.18	0.6	0.4?	–	0.8	13	–
B[2]	428	3400	3200	–	3120	3200	3200
Si[2]	170	68.5	70	–	36	33	35
Mn[2]	<0.1	0.03	0.01	–	0.03	0.01	0.01
Fe[2]	<0.2	2.26	2	–	1.5	0.9	2
NH_3^2	<0.1	332	220	–	240	270	220
$^{87}Sr/^{86}Sr$	0.7091	–	0.70535	–	–	–	0.70535
$d^{18}O$ (‰)	0	–	2.5	–	–	–	2.5
dD (‰)	0	–	12	–	–	–	12
U[3]	14.2	–	–	–	0.8	0.5	0.7
Mo[3]	115	–	–	–	–	1.1	–

[1]mmol/kg; [2]μmol/kg; [3]nmol/kg.

waters and discharge fluids as previously shown by Wheat et al. (2008). For example, distinct differences in the alkali metals exist (Table 1), likely attributed to sampling artifacts induced during the extraction of pore waters (e.g., De Lange et al., 1992). Similarly, extraction artifacts may influence the concentrations of dissolved silicon in pore waters, which are about twice the concentration of discharging fluids. The lower K, Rb, and Si and higher Li and Cs in the discharging fluids relative to pore waters affect previously described element/element ratios, which were used to constrain thermal conditions within the subduction channel (Hulme et al., 2010), and in the case of dissolved silicon also will impact models of silicate mineral stability.

Both stagnant and discharging fluids contained measurable amounts of formate and acetate with concentrations in the range of 6–40 μmol/kg. There were no systematic differences between the concentrations of these two organic acids between the two fluids types collected in 2009.

5. DISCUSSION

5.1. Chemical composition of two endmember fluids

Chemical characterization of pore waters, the stagnant fluid, and discharging fluids has revealed a range of sulfate concentrations; one that is sulfate rich, one that is low in sulfate and one with an intermediate sulfate concentration (Table 1). Mottl et al. (2003) suggested that the fluids characterized by a seawater sulfate concentration and the low sulfate solutions share a common origin at depth, but are

variably affected by microbial processes during transport towards the seafloor. In particular, as the deep-sourced, sulfate-rich fluid ascended from the subduction channel it experienced anaerobic oxidation of methane (AOM; e.g., Soetaert et al. 2007) by microbes at high pH to produce the shallow, low-sulfate fluid observed in the upper 17 mbsf at Hole 1200E (Mottl et al., 2003; Aoyama et al., 2018) according to the reaction:

$$CH_4 + SO_4^{2-} + OH^- => CO_3^{2-} + HS^- + 2H_2O \quad (1)$$

This reaction consumes methane and sulfate, lowers the pH through the consumption of hydroxide and increases alkalinity. The stoichiometry of reaction (1) indicates that for every mole of sulfate and methane consumed, a mole of sulfide is produced and the alkalinity increases by two molar equivalents due to the loss of a hydroxyl ion and the production of carbonate and hydrogen bisulfide. A similar reaction can be written with organic matter as the source of carbon;

$$2CH_2O + SO_4^{2-} + 3OH^- = 2CO_3^{2-} + HS^- + 3H_2O \quad (2)$$

where CH_2O represents complex organic matter containing nitrogen. Reaction (2) would have the same effect on sulfate, sulfide, and measured alkalinity as reaction (1); however, the effect on methane concentrations and pH would be different and would also result in elevated ammonia concentrations typically observed during degradation of complex organic matter (Froelich et al., 1979). Reaction (2) does not play a significant role at South Chamorro Seamount based on the low concentrations of ammonia in pore waters, which are too low for typical degradation of complex organic matter, and the measured difference in pH (25 °C) values between the sulfate-rich and low-sulfate pore waters cannot be accounted for by reaction (2) (Mottl et al., 2003). Furthermore, serpentinite material from below the upper 3 mbsf in South Chamorro Seamount is depleted in organic carbon (36 samples were <0.01 wt.% and the other 9 were >0.01 but <0.05 wt.%) (Mottl et al., 2003). Another potential reaction is the reduction of sulfate by dissolved hydrogen (Kawagucci et al., 2018); however, like reaction (2) this potential reaction is not consistent with observed changes in pH, alkalinity and methane concentrations.

As noted above, discharging fluids from Hole 1200C in 2003 and 2009 are similar in composition to the low-sulfate AOM-affected pore waters sampled in 2001 (Table 1). These fluids are assumed to be the same, with compositional differences resulting from handling artifacts induced during pore water extraction and mineral precipitation from dilution of the 2003 fluids with seawater. Given the almost identical composition of the discharging fluids from HPD945, 947, and 1007–1010 that were collected four months apart, we define the average of these fluids to represent the composition of the low sulfate fluid in the discussion that follows (Table 1). Assuming that the composition of this fluid is affected by reaction (1) and the composition of a deep-sourced fluid prior to AOM is represented by the sulfate-rich, pore water reported by Mottl et al. (2003), then the consumption of sulfate (~27.2 mmol/kg) should raise the measured alkalinity by ~54.4 mmol/kg to 116 mmol/kg, almost identical to the values measured in the low-sulfate discharging fluids (120 mmol/kg; Table 1 and Fig. 3). Similarly, the sulfide concentration would increase by ~27.2 mmol/kg, which is similar to the measured value of 24.8 mmol/kg in the low-sulfate discharging fluids (Fig. 3). The slightly lower values for the measured sulfide concentrations may reflect exposure to steel casing and screening materials that could potentially remove hydrogen sulfide as iron sulfide minerals. The stoichiometry of reaction (1) is consistent with the measured pH (25 °C) of 12.1 in the discharging fluid stemming from a deep-sourced, sulfate-rich fluid with a calculated pH (25 °C) of 12.4 (based on a calculated activity coefficient of 0.78 for H^+). The calculated pH (25 °C) is consistent with the value of 12.5 ± 0.1 measured in pore waters from the deep-sourced, sulfate-rich fluid (Table 1; Mottl et al., 2003). Given a methane concentration of 23 mmol/L in the low-sulfate, discharging fluid, the deep-sourced, sulfate-rich fluid should have a methane concentration of 50 mmol/L (Fig. 3). This value is substantially higher than the 2 mmol/L reported for the sulfate-rich, deep-sourced pore water (Mottl et al., 2003), likely reflecting extensive degassing that occurs during shipboard sample processing of volatile-rich sedimentary pore waters.

Comparison of the stagnant fluid composition with the low-sulfate, AOM-affected, discharging fluid and the deep-sourced, sulfate-rich pore water suggests that the stagnant fluid is a mixture of these two endmembers. If conservative mixing is assumed, the stagnant fluid with a sulfate concentration of 12.1 mmol/kg is a mixture containing 58% of the AOM-affected, low-sulfate fluid and 42% of the deep-sourced, sulfate-rich fluid (Fig. 3). Similar mixtures were calculated for the alkalinity data. The sulfide concentration in the stagnant fluid was 7.5 mmol/kg, substantially lower than 14.4 mmol/kg predicted for a 58:42 mixture, suggesting removal of sulfide within the mild-steel casing during the 6-year period that the stagnant fluid resided in the borehole. Loss of hydrogen sulfide cannot be

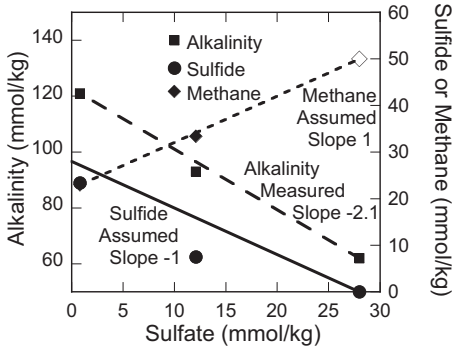

Fig. 3. Alkalinity (squares), sulfide (circles), and methane (diamonds) versus sulfate concentrations in fluids from Hole 1200C on South Chamorro Seamount. Filled symbols are measured data. The non-filled symbol represents calculated data. Lines show measured alkalinity trends with a slope of −2.1, similar to the theoretical value of 2 in reaction (1). In contrast, lines for sulfide and methane are theoretical and based on reaction (1). Symbols for the high-sulfide and low methane in the low sulfate fluid overlap.

attributed to homogeneous precipitation of metal sulfides from solution since no dissolved metals were present in sufficient concentrations to account for the observed depletions in hydrogen sulfide.

There are significant differences in the carbon isotopic composition of methane in the low-sulfate, discharging fluid ($\delta^{13}C_{CH4}$ of −37.4‰) and the stagnant fluid ($\delta^{13}C_{CH4}$ of −26.4‰). Based on the 58:42 mixing ratio calculated above, an isotopic mass balance yields a $\delta^{13}C_{CH4}$ value of −18.4‰ for dissolved methane in the deep-sourced, sulfate-rich fluid. This value is approximately 4‰ lighter than the value of −14.5‰ reported for pore water methane (Komor and Mottl, 2005), likely reflecting the extensive degassing of the pore waters and enrichment of ^{13}C in the residual dissolved methane due to kinetic isotope effects.

At first glance, depletion of ^{13}C in methane from AOM-affected, low-sulfate, discharging fluids may appear inconsistent with conventional isotopic systematics that predict enrichment of the heavier isotope in residual methane during degradation due to a kinetic isotope effect. However, field and laboratory studies have revealed ^{13}C depletions in residual methane during AOM when sulfate concentrations are low (Borowski et al., 1997; Hoehler et al., 2000, Pohlman et al., 2008; Yoshinaga et al., 2014). These isotopic depletions have been attributed to a small microbially induced backflux of methane under conditions of low sulfate activity that does not result in the net production of methane, but does facilitate carbon isotopic equilibrium and the production of ^{13}C-depleted methane (Yoshinaga et al., 2014). Accordingly, ^{13}C-depleted methane in the AOM-affected, low-sulfate, discharging fluids relative to the deep-sourced, sulfate-rich fluid are consistent with an active role for AOM in modifying the fluid's chemical composition.

5.2. Subsurface fluid flow and reservoirs

On the basis of the pore water data, Mottl et al., (2003) accounted for the measured chemical profiles at ODP Site 1200 by the upward seepage of a deep-sourced, sulfate-rich fluid that undergoes microbial AOM near the seafloor. This explanation is consistent with existing data at the time of publication. However, the data present some interesting conundrums. First, the effects of microbial alteration on pore water composition in sediments is minimized with faster pore water seepage (e.g., Wheat and McDuff, 1994; Wheat and Mottl, 1994; Wheat and Fisher 2008), thus why is the affect of AOM more prevalent in the faster upwelling fluid? Also, why is AOM restricted to the upper 17 m of the sediment column when all of the chemical components for possible AOM are present at deeper depths?

New data from 2009 allow us to develop an alternative model to account for ascending fluid composition within South Chamorro Seamount that considers the three dimensionality of the seamount. Our model involves a deep-sourced sulfate-rich fluid that ascends through multiple pathways to the summit (Fig. 4). Some pathways bisect environments that contain potential inoculum that ignites AOM, consuming sulfate, and producing the low-sulfate fluid that also vents at the seafloor. This model is constrained by the observation that (1) AOM must occur at depths below the upper 17 mbsf, (2) complex intertwined fluid pathways exist, and (3) a likely source of inoculum is located within the pelagic sedimentary layer that exists beneath serpentinite mud volcanoes (e.g., Fryer et al., 2018).

The low-sulfate pore waters in the upper 17 mbsf are similar to the discharging fluids. Such discharging fluids must enter the screened section of the borehole, which is ~70 m deeper than the deepest depth that pore waters were sampled at this site (Fig. 2A). Thus, discharging fluids, which enter the borehole through the screened section (148.8–202.3 mbsf), require a source that is at the depth of or deeper than the screened casing, because there is no reasonable mechanism to transport the low-sulfate fluid from the upper 17 mbsf to deeper depths in a hydrologic system that is positively pressure by ~170 kPa (Vinas, 2013).

Complex intertwined fluid pathways are included in our model given changes in the composition of borehole fluids. In 2003, Hole 1200C was left open for 37 days before a low-sulfate fluid was sampled (Wheat et al., 2008) (Fig. 2B). When we returned in 2009 (HPD941) the stagnant fluid in the borehole was a mixture of 58% low-sulfate, AOM-affected fluid and 42% deep-sourced, sulfate-rich fluid (Fig. 2C). When the borehole was allowed to discharge freely in 2009, low-sulfate fluids discharged (Fig. 2D). The existence of the stagnant fluid, which formed by conservative mixing of the two compositionally distinct fluids, point to two active hydrologic systems within the serpentinite mud volcano, one associated with the deep-sourced, sulfate-rich fluid and the other associated with a low-sulfate, AOM-affected fluid. This assertion of two active reservoirs is established because diffusion alone is not capable of producing the stagnant fluid, given that the nominal scale of molecular diffusion is <1 m during a 6-year period. Thus the composition of the stagnant fluid requires flow of the deep-sourced, sulfate-rich fluid through the screened section and thermally-driven convection and mixing within the borehole. This model requires the flow of the deep-sourced, sulfate-rich fluid through the screened section when the borehole is sealed and flow of the low-sulfate, AOM-affected fluid through the screened section when the borehole is open (Fig. 2).

A complex network of fluid pathways is consistent with the geologic structure of the seamount. The bathymetry of the knoll points to a central recently active conduit and the numerous arcuate, en echelon scarps on the summit region near the edge of apparent headwall scar that penetrates the southeastern side of the seamount summit are consistent with fluid pathways that are supported by the opening of fractures at depth that propagate toward the seafloor from the slip plane (Fig. 1; Wheat et al., 2008). Such listric faults may reach the pelagic sediment below the serpentinite mud volcano (Oakley et al., 2007) (Fig. 4). The number of visual scarps at the seafloor suggests that many potential fluid pathways exists, allowing, both the deep-sourced, sulfate-rich fluid (S351, Mottl et al., 2004) and the low-sulfate, AOM-affected pore waters (Mottl et al., 2003) to discharge

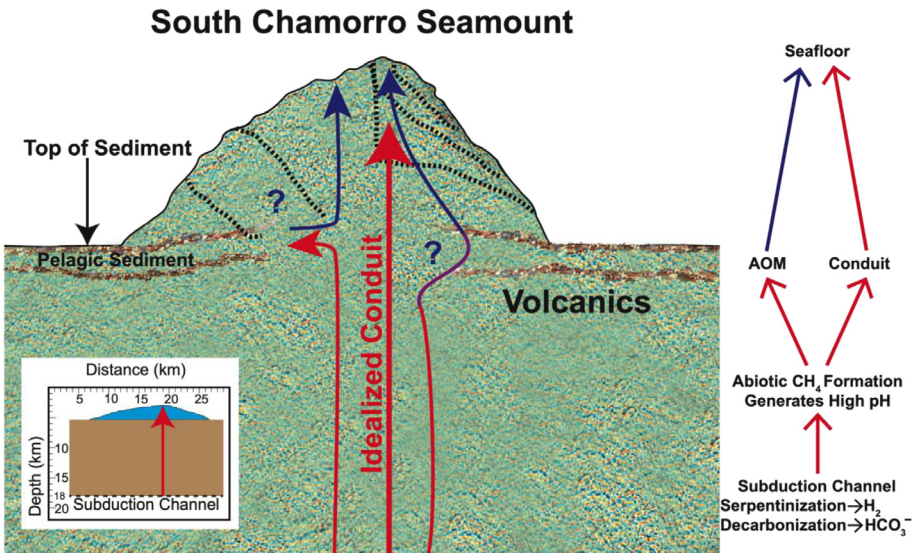

Fig. 4. Idealized pathways and potential reaction sites of deep-sourced, sulfate-rich fluids that ascend from the subduction channel. Such fluids may discharge at the seafloor unaltered via the central conduit, react during ascent with pelagic sediment before discharging as a low-sulfate, AOM-affected fluid, or ascend and mix within the pelagic sediment layer and later discharge at the seafloor in response to a change in the subsurface pressure regime. This diagram was modified from data for other serpentinite mud volcanoes to illustrate the potential reaction zone for AOM (Oakley et al., 2007). The inset shows the seamount shown to scale in context to the depth to the subduction channel (~18 km, Oakley et al., 2008).

at the seafloor. The observed seepage, based on the pore water and fluid chemical data, at both of these sites and on the summit knoll in general, provide a snapshot of current conditions. However, current fluid flow conditions cannot the transport large boulders that are suspended within the serpentinite mud matrix, requiring a temporal (e.g., seismic) component to discharge (Fryer et al., 1990; Phipps and Ballotti, 1992; Fryer, 2012).

Below the base of the serpentinite mud volcano we suggest that both fluids originate from a single deep-sourced, sulfate-rich fluid that ascends a central conduit prior to reaching the pelagic sediment that underlies the serpentinite mud volcano. Temperatures within the subduction channel below South Chamorro Seamount are in excess of the thermal limits of life (250–350 °C, Alt and Shanks, 2006; Debret et al., 2019; Gharib, 2006, Hulme et al., 2010). As these sterile sulfate-rich fluids ascend a likely depth horizon that could provide inoculum is the pelagic sediment that underlies serpentine mud volcanoes. Seismic data reveal pelagic sediment under each of the serpentinite mud volcano that have been surveyed (South Chamorro Seamount was not surveyed, Oakley et al., 2007) and pelagic sediment was recovered from Fantangisña (Celestial) Seamount during IODP Expedition 366 (Fryer et al., 2018). Because buried pelagic sediment was once in contact with overlying seawater, it may harbor microbes capable of AOM that were subsequently stimulated by upwelling fluids containing abundant sulfate and methane at temperatures elevated from bottom seawater temperatures (15–90 °C, assuming the pelagic sediment is 1250 m below the summit, Salisbury et al., 2002), but in the temperature range of known microbial life. Furthermore these pelagic sediments contain a significant portion of volcanic ash (e.g., Fryer et al., 2018), which could supply nutrients (e.g., phosphate) and/or bioavailable metals (e.g., Cu, Fe, Mo, Ni, Co, and Zn) to aide in microbial AOM (e.g., Glass and Orphan, 2012).

Within the context of this model, the presence or absence of AOM in upwelling fluids at the seafloor may reflect the extent to which the deep-sourced fluids have interacted with pelagic sediment (Fig. 4). For example, flow through the central conduit may have flushed out pre-existing pelagic sediments, allowing sterile, sulfate-rich fluids to reach the seafloor without undergoing AOM. In contrast, other paths for fluid flow may intersect pelagic sediment, during ascent of fluids from the subduction channel to the seafloor, resulting in the low-sulfate fluid. Another possibility is that the deep-sourced, sulfate-rich fluid percolates within the pelagic sediment beneath the mud volcano. This fluid "stews" and is subsequently flushed out in response to tectonic forces or changes in the structure of the seamount. For example, if the borehole discharged fluid at 0.1 L sec^{-1} for 1000 days, then $\sim 9 \times 10^6$ L discharged during this period. This volume is ~1% of the volume represented by a cylinder with a diameter of 50 m and a length of 500 m, which is the minimal sediment thickness in the Mariana forearc (Oakley et al., 2008). Such a small decrease in the pore space volume at depth could be induced from the additional overburden from material that formed the new summit knoll, which is ~200 m in height, or from forces in response to gravitational deformation (Oakley et al., 2007).

Our model is consistent with the pore water data if we consider a three dimensional scenario. We suggest that Hole 1200E bisected a non-vertical hydrologic zone in a complex hydrologic setting that discharges low-sulfate fluid

and the deep-sourced, sulfate-rich fluid, which discharges throughout a larger area of the summit knoll than the low-sulfate fluid. In terms of the pore water chemical profile at Hole 1200E, the initial 17 mbsf represents the vertical transport of the low-sulfate fluid from depth (e.g., the pelagic layer below the serpentinite mud volcano), the depth zone from ~17 to 30 mbsf represents a conservative mixing zone between sulfate-rich and low-sulfate fluids and the zone deeper than 30 mbsf represents the transport of the deep-sourced, sulfate-rich fluid. In terms of other dissolved ions such as Na, Cl, K, Mg, Ca, Li, Rb, Cs, Sr, Si, and B, pore water profiles in one dimension would be consistent with the uniform upwelling of a deep-sourced fluid, because the deep-sourced and low-sulfate, discharging fluids have identical concentrations for these ions (Table 1).

5.3. Origin of Deep-Sourced Fluid Composition

The formation of serpentinite materials that form the Mariana forearc mud volcanoes results from the reaction of water derived from the downgoing Pacific Plate with ultramafic olivine-rich rocks composed mostly of harzburgite in the overlying Philipine Plate. In general, serpentinization of harzburgite involves the hydration of olivine and orthopyroxene to produce magnetite, serpentine, brucite, dissolved hydrogen, and alkaline fluids (e.g., Bach et al., 2006). Temperature and rock composition influence the pH value of the fluid, which is buffered by secondary minerals (Palandri and Reed, 2004; Klein et al., 2013). For example, equilibrium models of serpentinization of Ca-free peridotite and pyroxenite produces *in situ* pH values that range from 9 to 4.5 at temperatures of 25–400 °C, respectively (Palandri and Reed, 2004; Klein et al., 2013). In contrast, *in situ* pH values estimated for serpentinization of Ca-bearing ultramafic lithologies range from 12 to 6 at temperatures of 25–400 °C, respectively (Palandri and Reed, 2004; Klein et al., 2013). This range in pH values is consistent with natural waters from serpentinite (pH (25 °C) of 10.7–11.8, Palandri and Reed, 2004) and ultramafic-hosted hydrothermal system (pH (25 °C) of 11, Kelley et al., 2005).

To facilitate comparison of the measured pH (25 °C) of the deep-seated sulfate-rich fluids at South Chamorro Seamount with *in situ* pH values estimated from thermodynamic models for serpentinization of ultramafic rocks at elevated temperatures, we calculated the *in situ* pH for the deep-seated, sulfate-rich fluid from 25° to 350 °C, using the fluid speciation and reaction path program EQ3NR/EQ6 version 8.0 (Wolery, 1992). For these calculations, only the aqueous phase was considered and mineral precipitation and redox reactions were suppressed. The supporting thermodynamic database for these calculations was generated at 50 MPa using SUPCRT92 software (Johnson et al., 1992) that included thermodynamic data for minerals (Helgeson et al., 1978) and relevant aqueous inorganic species (Shock and Helgeson, 1988; Shock et al., 1989, 1997; Sverjensky et al., 1997). Fig. 5 reveals a decrease in the *in situ* pH values for the deep-seated fluid from the measured pH value of 12.5 at 25 °C to values near 10 at temperatures greater than 200 °C. These pH values are substantially greater than the maximum range of *in situ* pH values estimated by Klein et al. (2013) for serpentinization of clinopyroxene-bearing harzburgite Thus, although serpentinization represents an effective means to generate highly alkaline fluids at low temperatures, it cannot account for the extraordinarily high pH levels observed in discharging fluids from South Chamorro Seamount.

As noted above serpentinization reactions also produce dissolved H_2. Hydrogen is produced through the oxidation of ferrous iron in the fayalite components of olivine and pyroxenes to the ferric iron components of magnetite and serpentinite. In general, greater ferrous iron contents in unaltered ultramafic rocks contribute to higher H_2 production (Klein et al., 2013). The production of H_2 is also dependent on water/rock ratios during fluid-rock interactions and pressure and temperature conditions. Temperatures of 250–350 °C are estimated for the ~18 km depth of the subduction channel below South Chamorro Seamount (Oakley et al., 2008; Alt and Shanks, 2006; Debret et al., 2019; Gharib, 2006; Hulme et al., 2010). Many laboratory experiments have demonstrated the rapid generation of H_2 during serpentinization of olivine and ultramafic rocks at 200–400 °C (Berndt et al., 1996; McCollom and Seewald, 2006; Allen and Seyfried, 2003; Seyfried et al., 2007; Klein and McCollom, 2013; Klein et al., 2015; Grozeva et al., 2017; McCollom, 2016; McCollom et al. 2016). The amount of H_2 produced reacting 0.5 M NaCl solution with olivine at 300 °C and 500 bars with a water-to-rock ratio of 2.25 was 158 mmol/kg after ~1700 hours (Berndt et al., 1996). During this experiment the trajectory of H_2 generation was increasing with experimental time, suggesting even greater H_2 concentrations could be generated (Berndt et al., 1996). Thermodynamic models predict even higher H_2 concentrations (Klein et al., 2009, 2013; McCollom and Bach, 2009). Thus, the conspicuously low concentrations of H_2 in the discharging fluids require H_2 consumption at depths below the screened portion of the borehole.

In contrast to the lower than expected dissolved H_2 concentrations, dissolved methane is abundant (50 mmol/L) in the deep-sourced, sulfate-rich fluids beneath South Chamorro Seamount. Potential sources for this high methane concentration include methane hydrates, organic-rich sediment, thermogenic production, and abiotic formation from carbonate species during subduction and/or upwelling. Neither gas hydrates nor microbial activity within an organic-rich sediment are consistent with the composition of the organic-lean sediment on the incoming Pacific Plate (Lancelot et al., 1990). Furthermore, the isotopic composition of methane calculated for the deep-sourced, sulfate-rich fluid ($\delta^{13}C = -18.4‰$, Table 1) is significantly enriched in ^{13}C relative to methane typically produced by sedimentary microbial methanogenesis that typically has $\delta^{13}C$ values less than −45‰ (Schoell, 1980; Whiticar, 1999). Thermogenic methane production is possible, given estimated temperatures of 250–350 °C in the down-going slab at South Chamorro Seamount; however, the carbon isotopic composition of methane in the deep-sourced fluid is more ^{13}C-enriched than methane generated by thermal maturation of marine or terrestrial organic matter that is

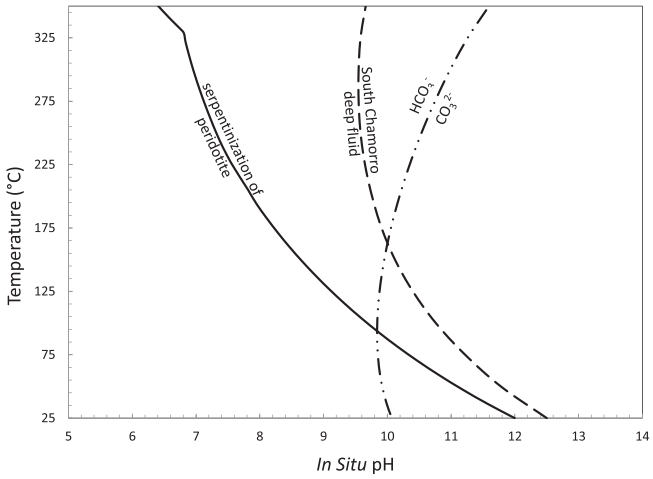

Fig. 5. Temperature dependence of the *in situ* pH of aqueous fluids during serpentinization of peridotite as calculated by Klein et al. (2013) (solid line), the *in situ* pH of the deep-sourced sulfate-rich fluid at South Chamorro Seamount, and the pK_a for the dissociation of HCO_3^- to CO_3^{2-}. The *in situ* pH of the South Chamorro Seamount fluids is greater than can be produced by serpentinization at all temperature shown and places the fluids in the stability field for HCO_3^- at temperatures greater than 175 °C. See text for details of the speciation calculations and thermodynamic necessary to construct this diagram.

characterized by $\delta^{13}C$ values of −45 to −20‰ (e.g., Schoell, 1980; Whiticar, 1999). In contrast, the $\delta^{13}C$ value of the deep-sourced fluid is entirely consistent with $\delta^{13}C$ values of −20 to −2‰ for methane attributed to abiotic synthesis in a variety of geological environments (Etiope and Sherwood Lollar, 2013).

We recognize that the subduction channel is a complex mixture of minerals, alteration products and rocks, but for simplicity we present idealized reactions that are consistent with the fluid data. To account for the high measured pH values, the lower than expected H_2, and high methane concentrations in the deep-sourced fluid from the subduction channel beneath South Chamorro Seamount, we suggest that methane forms abiotically from HCO_3^-, according to the reaction:

$$4H_2 + HCO_3^- == CH_4 + 2H_2O + OH^- \quad (3)$$

where H_2 is generated by serpentinization and HCO_3^- is derived from dissolution of subducted carbonate (i.e., decarbonization; Fryer et al., 1999; Mottl et al., 2004; Hulme et al., 2010). Reaction (3) conserves alkalinity; however, bicarbonate alkalinity is replaced with hydroxide alkalinity, resulting in an increase in pH. Thus, reaction (3) represents an effective mechanism to generate hydroxide concentrations in the deep-sourced fluids beneath South Chamorro Seamount that exceed values produced by serpentinization reactions. In addition, because each mole of methane produced consumes four moles of H_2, production of 50 mmol/L methane requires consumption of 200 mmol/kg H_2, implying that serpentinization reactions may have contributed substantial amounts of H_2 to the deep-sourced fluids during their early history, consistent with experimental and theoretical studies mentioned above. Thus, given a temperature of ~250–350 °C in the subduction channel below South Chamorro Seamount (Maekawa et al., 1993; Alt and Shanks, 2006; Debret et al., 2019; Gharib, 2006; Hulme et al., 2010), thermodynamic calculations would predict water-rock mass ratios < 2, based on the estimated H_2 concentrations prior to abiotic methane formation (Klein et al., 2009).

Methane formation from HCO_3^- according to reaction (3) is thermodynamically favorable at temperatures below 350 °C when the *in situ* pH is buffered to values below 12 and H_2 concentrations are greater than 1 mM (Fig. 6). Because serpentinization reactions buffer pH to values below 12 (Klein et al., 2013) and result in the production of H_2 at concentrations substantially greater than 1 mM (Berndt et al., 1996; McCollom and Seewald, 2006; Allen and Seyfried, 2003; Seyfried et al., 2007; Klein and McCollom, 2013; Klein et al., 2015; Grozeva et al., 2017; McCollom, 2016; McCollom et al. 2016), reduction of HCO_3 will proceed until one of the reactants approaches a near zero concentration, assuming there are no kinetic barriers.

A process similar to reaction (3) involving CO_3^{2-} instead of HCO_3^- and producing two moles of OH^- for each mole of methane formed was proposed by Mottl (2009) as a mechanism to increase the pH of fluids at South Chamorro Seamount. However, at temperatures above 100 °C, HCO_3^- becomes a weaker acid and is increasingly stable at higher pH values (Fig. 5). Thus, at *in situ* pH values regulated by serpentinization above ~175 °C, HCO_3^- is the thermodynamically stable aqueous carbonate species. A further indication that reaction (3) is responsible for methane production is provided by the composition of the deeply sourced upwelling fluids. Based on the stoichiometry of reaction (3), production of 50 mmol/kg CH_4 will produce an equivalent concentration of OH^-. This amount of OH^- exceeds the amount of hydroxide alkalinity that can be produced by serpentinization reactions at elevated temperatures (Klein et al., 2013) by more than an order of magnitude and results in a measured pH (25 °C) of 12.4

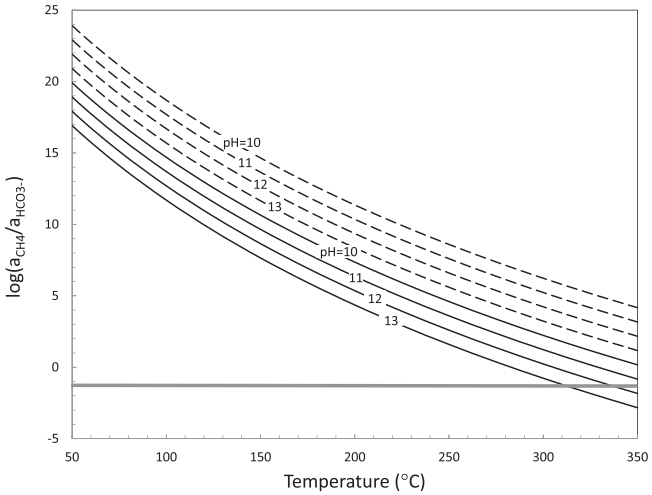

Fig. 6. Semi-log plot showing the activity ratio of dissolved methane and HCO_3^- in equilibrium with dissolved H_2 concentrations of 1 mmol/L (solid lines) and 10 mmol/L (dashed lines) as a function of temperature and pH at 500 MPa. For H_2 concentrations greater than 1 mmol/L activity ratios are greater than unity, indicating formation of methane from HCO_3^- is thermodynamically favorable. See text for details of the speciation calculations and thermodynamic necessary to construct this diagram.

after accounting for activity coefficients and aqueous complexing. The latter value is almost identical to the measured pH (25 °C) of the deep-sourced, sulfate-rich fluid from South Chamorro Seamount (12.5, Table 1).

Decarbonization of the downgoing plate has been postulated based on observations from a number of serpentinite mud volcanoes that revealed systematic trends in measured pH values and Ca and alkalinity concentrations as a function of distance from the trench (Fryer et al., 1999; Mottl et al., 2004; Hulme et al., 2010) (Table 2). For example, near the trench, where the subduction channel is shallower and cooler, pore waters have high Ca and low alkalinity concentrations with pH (25 °C) values <11. In contrast, serpentinite mud volcanoes that are farther from the trench (e.g., Asùt Tesoro (Big Blue), South Chamorro, and Conical Seamounts), where the subduction channel is deeper and warmer, have pH (25 °C) values of 12.5 with depleted Ca and enriched alkalinity concentrations. The source of carbonate likely stems from the increase in calcite solubility with temperature at pressures greater than 0.3 GPa (~10–12 km depth) (Caciagli and Manning, 2003).

Dissolution of calcite results in the release of one mole of Ca for each mole of carbon. Because deep-sourced fluids from South Chamorro Seamount have low (<0.2 mmol/kg) concentrations of dissolved Ca, Ca removal is likely buffered by Ca-bearing secondary minerals. Seyfried et al. (2007) have shown that hydrothermal alteration of peridotite during laboratory experiments removes Ca as Ca-bearing alteration minerals. They attribute the decreasing solubility of Ca phases during continued reaction to increasing *in situ* pH that results from incongruent dissolution of the Na_2O component of clinopyroxene, according to the reaction:

$$Na_2O_{(cpx)} + H_2O = 2Na^+ + 2OH^- \quad (4)$$

Table 2
Selected properties of serpentinite mud volcanoes in the Mariana forearc and fluid concentrations of selected analytes in the deep-sourced fluid. Data are from Oakley et al. (2008), Hulme et al. (2010), and Wheat et al. (2018).

Seamount	Distance to trench km	Depth to Slab km	pH	Ca mmol/kg	Alkalinity mmol/kg	Na/Cl molar ratio
Bottom seawater			8.1	10.2	2.3	0.86
Blue Moon	55	13	10.7	58	1.4	0.78
Cerulean Springs	60	14	10.8	49.5	2.3	0.72
E Quaker	61	14	10.7	74.8	3.1	0.72
Celestial	62	14	~10.8	>82	<0.5	0.87
NE Quaker	63	15	>8.3	>33	<1.3	<0.86
Pacman Summit	70	17	>8.9	<6.9	<1	0.89
Quaker	76	18	9.2	18.1	0.8	1.08
Baby Blue	72	18	>9	<6.9	<1	>0.93
Big Blue	72	18	12.5	0.1	73	1.19
S. Chamorro	78	18	12.5	0.3	62	1.20
Conical	86	19	12.5	1	52	1.50

The increase in pH induces aqueous Ca removal from solution by shifting the equilibrium of Ca-bearing mineral assemblages. For example, combining the pH dependent equilibration of epidote and lawsonite, two stable minerals at the temperatures and pressures encountered by the subducting slab (Maekawa et al., 1992; Maekawa et al., 1995; Mottl, 2009), with reaction (4) yields the overall reaction:

$$\underset{\text{Lawsonite}}{3CaAl_2Si_2O_7(OH)_2.H_2O} + Ca^{2+} + Na_2O(cpx) = \underset{\text{epidote}}{2Ca_2Al_3(SiO_4)_3(OH)} + 5H_2O + 2Na^+ \quad (5)$$

The net effect of reaction (5) is the pH independent aqueous exchange of Ca for Na. A similar pH independent exchange can be written for the precipitation of portlandite as follows:

$$Ca^{2+} + Na_2O(cpx) + H_2O = Ca(OH)_2 + 2Na^+ \quad (6)$$

Reactions (5) and (6) increase the aqueous concentration of Na. Assuming that the Na/Cl molar ratio is initially set by pore water and formation fluids from the subducting plate, Na increases in the deep-sourced fluids at South Chamorro Seamount are indicated by high measured Na/Cl molar ratios (1.2) compared to seawater (0.86). The observed Na/Cl ratio at South Chamorro Seamount requires the addition of 177 mmol Na/kg after accounting for the decrease from seawater chloride concentrations (538 mmol/kg) to the measured chloride concentration of 510 mmol/kg in the deep-sourced fluid, and assuming the fluids initially had a seawater Na/Cl molar ratio of 0.86 (Tables 1 and 2). Addition of 177 mmol/kg Na to solution by reactions (5) or (6) would require the removal of 88.5 mmol/kg aqueous Ca. The latter value is remarkably similar to the total carbon content of the deep-sourced fluid consisting of 46 mmol/kg from carbonate alkalinity (Mott et al., 2004) and 50 mmol/L methane, consistent with a carbon source from the dissolution of carbonate in the subducted slab.

The model presented above can account for the low measured H_2 concentration and the high pH values, methane concentrations, and high Na/Cl molar ratios of the deep-sourced, sulfate-rich fluid beneath South Chamorro Seamount. Other serpentinite mud volcanoes (Asùt Tesoro (Big Blue) and Conical Seamounts) have similar pH, Ca, and Na/Cl molar values in their deep-sourced fluid (Table 2), implying that similar decarbonazation and Ca removal reactions occur beneath them. In contrast, serpentinite mud volcanoes that are closer to the trench, and by inference overlying a shallower and cooler portion of the subduction channel, have high Ca and low alkalinity concentrations and pH values in the range of 9–11 (Table 2). These lower pH fluids are derived from serpentinization reactions, but are unaffected by abiotic methane production. In the context of such a model, the near-trench, deep-sourced fluids should have pH values of 9–11 (Table 2), be depleted in dissolved abiotic methane, and enriched in dissolved H_2, barring microbial mediated consumption. Here microbial sulfate reduction could occur with methane derived from biotic sources and other pathways that include dissolved H_2.

6. IMPLICATIONS

The model presented above has implications for the extent of serpentinization and production of abiotic methane in the subduction channel, microbial activity and metabolic pathways, and mass balances of water and materials in an active serpentinite mud volcano. The model can used to assess biogeochemical processes at three new boreholes that were installed during IODP Expedition 366, at Yinazao (Blue Moon; Hole U1492D), Fantangisña (Celestial; Hole U1497D), and Asùt Tesoro (Big Blue; Hole U1496C) Seamounts (Fryer et al., 2018) (Table 2). Each of these boreholes was sealed with cement at the bottom and included a screened portion of casing, similar to the configuration of Hole 1200C at South Chamorro Seamount. A few days after deploying the cement, the expedition returned to Fantangisña (Celestial; Hole U1497D) and Asùt Tesoro (Big Blue; Hole U1496C) Seamounts to assess the status of the cement plug and collect a water sample (Fryer et al., 2018). Both samples included a component of the formation fluid, indicating that the hydrologic system was rebounding and active flow of serpentinite-sourced fluids discharged into the borehole; however, the fraction of the deep-sourced fluid was difficult to quantify (Fryer et al., 2018). Given that the samples were collected in non-gas-tight samplers, the boreholes were rebounding from drilling disturbances, and there is evidence for current brucite and carbonate mineral precipitation within the borehole, it is unlikely that the measured concentrations of methane and H_2 reflect values in the discharging fluid. Because molar ratios of H_2/CH_4 are less affected by these issues, they may be representative of discharging fluid. The sample from Fantangisña (Celestial) Seamount (Hole 1497D), located closer to the trench than South Chamorro Seamount, had a H_2/CH_4 of 50, suggesting the presence of an H_2-rich and CH_4-poor fluid. This conclusion coupled with a pH (25 °C) < 11 and high Ca concentration is consistent with a fluid that is regulated by serpentinization reactions without the effects of abiotic methane formation (Table 2). In contrast, a H_2/CH_4 value of 3.6 was measured in the sample from Asùt Tesoro (Big Blue) Seamount (Hole U1496C), located further from the trench than Fantangisña (Celestial) Seamount (Hole 1497D) but closer than South

Chamorro Seamount, where upwelling pore waters have a pH (25 °C) of 12.5 and low Ca concentration, similar to fluids that discharge from South Chamorro Seamount and consistent with abiotic methane formation within the subduction channel beneath Asùt Tesoro (Big Blue) seamount. Although these initial data are not definitive, they provide evidence that methane formation by reaction (3) and decarbonazation play an increasing role in regulating the composition of fluids derived from the subduction channel as temperatures and pressures rise during descent of the Pacific Plate.

Our model suggests that the permeable conduits could bring sterile fluids and materials from the subduction channel to the surface of South Chamorro Seamount. Because flow paths are complex due to geologic heterogeneity, some pathways may bisect the pelagic sediment underlying the serpentinite structure. Here, deep-sourced, sulfate-rich fluids may undergo AOM. Studies have shown microbes can tolerate high pH fluids (Takai et al., 2001, 2005: Kelley et al., 2005; Brazelton et al., 2006; Curtis et al., 2013; Kawagucci et al., 2018) and assimilate methane, acetate, and formate (Kawagucci et al., 2018). Kawagucci et al (2018) determined methane assimilation rates under anaerobic conditions of 0.039 nmol day^{-1} L^{-1} with "pelagic" microbes in fluids that discharged from the borehole at South Chamorro Seamount. It is not surprising that the fluid composition in the stagnant fluid was not modified by microbial activity because only 83 nmol CH_4/L would have been consumed in 6 years. Furthermore, at this rate it would take 2 million years to produce the low-sulfate, AOM-affected fluid. A 2 million-year-old reservoir is not out of the question for this geologic setting, given that serpentinite mud volcanoes have been active in the Mariana forearc for 50 million years (Fryer et al., 2000), but the combination of the increase in temperature at depth and the potential contribution from microbial communities that live on mineral surfaces likely would decrease the time required to consume sulfate in the deep-sourced fluid. Although much of our discussion has focused on AOM, it is not the only potential metabolic pathway; acetate and formate also are present in these fluids. Experimental assimilation rates of acetate (0.004 nmol day^{-1} l^{-1}) and formate (0.06 nmol day^{-1} l^{-1}) are low (Kawagucci et al., 2018). With such low rates only 0.13 μM formate or 0.001 μM acetate would be consumed in six years in the stagnant fluid. Given the 58/42 mixture presented above the deep-sourced, sulfate-rich fluid would have a larger formate and lower acetate concentration than the low-sulfate, AOM affected fluid, suggesting that microbial metabolic pathways or abiotic reactions consume formate while producing acetate. Systematic sampling from this and additional serpentinite mud volcanoes is needed to resolve subsurface reactions for these constituents.

With our estimate for the dissolved H_2 concentration in the subducting slab coupled with experimental data, we can begin to constrain water to rock ratios, leading to a better understanding of mass balances of water and materials in an active serpentinite mud volcano and in the subduction channel. The minimum mass of serpentinite material created is defined by bathymetric data and assuming a porosity profile with depth. This overall mass is made from numerous eruptive events. In addition to this mass flux, fluids discharge at a rate that is in excess of the serpentinite matrix. In general, pore waters in serpentinite mud volcanoes ascend at rates that are several to tens of cm y^{-1} faster than the surrounding mud matrix with the fastest seepage rate of 36 cm y^{-1} in this setting (Fryer et al., 1999; Mottl et al., 2003, 2004; Hulme et al., 2010). However, such a slow seepage rate cannot maintain the presence of boulders within the serpentinite mud matrix (Phipps and Ballotti, 1992), requiring another transport mechanism that is likely triggered by intermittent events with high discharge rates. Such a high discharge that minimizes the residence time of materials at depth is further supported by observations of prograde metamorphic effects on the metabasites, implying the ascent of these materials must be fast to minimize alteration in such a highly reactive fluid environment (e.g., Fryer et al., 2006, 2018). Such eruptive events are currently poorly constrained; however, knowledge of the water to rock ratio in the subduction channel will place constraints on the potential viscosity of such flows. Higher water to rock ratios could mean more fluidized serpentinite material characteristic of 18-km-long thin flows (Fryer and Mottl, 1992) and other "braded" flows on serpentinite seamounts that are more distal from the trench (Fryer et al., 2018), whereas lower water to rock ratios may produce more viscous mud flows typical of those observed on Fantangisña (Celestial) Seamount, which is closer to the trench (Fryer et al., 2018).

ACKNOWLEDGEMENTS

The authors thank the entire shipboard parties of cruises NT09-01 and NT09-07 on the *R/V Nastushima* and the crews and pilots of the ROV *HyperDolphin*. We also thank Tom Pettigrew for removing the dummy plug and designing the insert for the borehole. This research was supported by the National Science Foundation (OCE-0727120 and 1439564 (CGW) and OCE--0725204 (JS)) and the Japan Agency for Marine-Earth Science and Technology. This is C-DEBI contribution 497.

APPENDIX A. SUPPLEMENTARY MATERIAL

Supplementary data to this article can be found online at https://doi.org/10.1016/j.gca.2019.10.037.

REFERENCES

Allen D. E. and Seyfried, Jr, W. E. (2003) Compositional controls on vent fluids from ultramafic-hosted hydrothermal systems at mid-ocean ridges: an experimental study at 400 C, 500 bars. *Geochim. Cosmochim. Acta* **67**(8), 1531–1542.

Alt J. C. and Shanks W. C. (2006) Stable isotope compositions of serpentinite seamounts in the Mariana forearc: serpentinization processes, fluid sources and sulfur metasomatism. *Earth Planet. Sci. Lett.* **242**(3), 272–285.

Aoyama S., Nishizawa M., Miyazaki J., Shibuya T., Ueno Y. and Takai K. (2018) Recycled Archean sulfur in the mantle wedge of the Mariana Forearc and microbial sulfate reduction within an extremely alkaline serpentine seamount. *Earth Planet. Sci. Lett.* **491**, 109–120.

Bach W., Paulick H., Garrido C. J., Ildefonse B., Meurer W. P. and Humphris S. E. (2006) Unraveling the sequence of serpentinization reactions: petrography, mineral chemistry, and petrophysics of serpentinites from MAR 15 N (ODP Leg 209, Site 1274). *Geophys. Res. Lett.* **33**(13).

Berndt M. E., Allen D. E. and Seyfried, Jr, W. E. (1996) Reduction of CO2 during serpentinization of olivine at 300 C and 500 bar. *Geology* **24**(4), 351–354.

Bloomer S. H. and Hawkins J. W. (1987) Petrology and geochemistry of boninite series volcanic rocks from the Mariana trench. *Contrib. Miner. Petrol.* **97**(3), 361–377.

Borowski W. S., Paull C. K. and Ussler, III, W. (1997) Carbon cycling within the upper methanogenic zone of continental rise sediments: an example from the methane-rich sediments overlying the Blake Ridge gas hydrate deposits. *Mar. Chem.* **57**, 299311.

Brazelton W. J., Schrenk M. O., Kelley D. S. and Baross J. A. (2006) Methane-and sulfur-metabolizing microbial communities dominate the Lost City hydrothermal field ecosystem. *Appl. Environ. Microbiol.* **72**(9), 6257–6270.

Caciagli N. C. and Manning C. E. (2003) The solubility of calcite in water at 6–16 kbar and 500–800°C. *Contrib. Miner. Petrol.* **146** (3), 275–285.

Chen C., Ogura T., Hirayama H., Watanabe H. K., Miyazaki J. and Okutani T. (2016) First seep-dwelling Desbruyeresia (Gastropoda: Abyssochrysoidea) species discovered from a serpentinite-hosted seep in the Southeastern Mariana Forearc. *Molluscan Res.* **36**(4), 277–284.

Curtis A., Wheat C. G., Fryer P. and Moyer C. (2013) Mariana forearc serpentinite mud volcanoes harbor novel communities of extremophilic *Archaea*. *Geomicrobiol. J.* **30**, 1–12. https://doi.org/10.1080/01490451.2012.705226.

Davis, E. E., Becker, K., Pettigrew, T., Carson, B., MacDonald, R. (1992) CORK: a hydrologic seal and downhole observatory for deep-ocean boreholes, In Proc. ODP, Init. Repts (eds. E. E. Davis, M. J. Mottl, A. T. Fisher, et al.) 139. College Station, TX (Ocean Drilling Program), pp. 43–53.

Debret B., Albers E., Walter B., Price R., Barnes J. D., Beunon H., Facq S., Gillikin D. P., Mattielli N. and Williams H. (2019) Shallow forearc mantle dynamics and geochemistry: new insights from IODP Expedition 366. *Lithos* **326**, 230–245.

De Lange, G. J., Cranston, R. E., Hydes, D. H. and Boust, D. (1992). Extraction of pore water from marine sediments: a review of possible artifacts with pertinent examples from the North Atlantic. In The Geochemistry of North Atlantic Abyssal Plains (Eds. J.J. Middelburg and S. Nakashima). Mar. Geol., 109, 53–76.

Etiope G. and Sherwood Lollar B. (2013) Abiotic methane on Earth. *Rev. Geophys.* **51**(2), 276–299.

Froelich P. N., Klinkhammer G. P., Bender M. L., Luedtke N. A., Heath G. R., Cullen D., Dauphin P., Hammond D., Hartman B. and Maynard V. (1979) Early oxidation of organic matter in pelagic sediments of the eastern equatorial Atlantic: suboxic diagenesis. *Geochim. Cosmochim. Acta* **43**, 1075–1090.

Fryer, P. (1992). A synthesis of Leg 125 drilling of serpentine seamounts on the Mariana and Izu-Bonin forearcs. In Scientific results, Ocean Drilling Program (eds. P. Fryer, J. A. Pearce, P. Coleman, L. B. Stokking), Leg 125. College Station, Texas, Ocean Drilling Program, p. 593–614.

Fryer P. (2012) Serpentinite mud volcanism: observations, processes, and implications. *Ann. Rev. Mar. Sci.* **4**, 345–373.

Fryer, P. and Fryer G. J. (1987). Origins of non-volcanic seamounts in a forearc environment. In Seamounts Islands and Atolls, (eds. B. H. Keating, P. Fryer, R. Batiza, and G. W. Boehlert), Geophys. Monogr. Ser., 43, 61–72, Washington, Am. Geophys. Un.

Fryer, P. and Mottl, M. J. (1992). Lithology, mineralogy, and origin of serpentine muds recovered from Conical and Torishima forearc seamounts: results of Leg 125 drilling. In Proc. Ocean Drill. Program Sci. Results (Vol. 125, pp. 343–362).

Fryer P. and Mottl M. J. (1997) Shinkai 6500 investigations of a resurgent mud volcano on the southeastern Mariana forearc. *JAMSTEC J. Deep Sea Res.* **13**(1997), 103–114.

Fryer, P., Pearce, J. A.,Stokking, L. B., et al. (1990). Proc. ODP, Init. Repts., 125. College Station, TX (Ocean Drilling Program).

Fryer P., Wheat C. G. and Mottl M. J. (1999) Mariana blueschist mud volcanism: implications for conditions within the subduction zone. *Geology* **27**(2), 103–106.

Fryer, P., Lockwood, J., Becker, N., Todd, C., and Phipps, S. (2000). Significance of serpentine and blueschist mud volcanism in convergent margin settings. In Ophiolites and Oceanic Crust: New Insights from Field Studies and Ocean Drilling (eds. Y. Dilek, E. M. Moores, D. Elthon, A. Nichols). Program. GSA SPE, 349, pp. 35–51.

Fryer P., Gharib J., Ross K., Savov I. and Mottl M. J. (2006) Variability in serpentinite mudflow mechanisms and sources: ODP drilling results on Mariana forearc seamounts. *Geochem. Geophys. Geosyst.* **7**(8).

Fryer, P., Wheat, C. G., Williams, T., and the Expedition 366 Scientists (2018). Mariana Convergent Margin and South Chamorro Seamount. In Proceedings of the International Ocean Discovery Program, 366. College Station, TX (International Ocean Discovery Program). https://doi.org/10.14379/iodp.proc.366.2018.

Gharib, J. (2006). Clastic Metabasites and Authigenic Minerals within Serpen- tinite Protrusions from the Mariana Forearc: Implications for Sub-Forearc Subduction Processes, University of Hawi, Honolulu, p. 239.

Glass J. and Orphan V. J. (2012) Trace metal requirements for microbial enzymes involved in the production and consumption of methane and nitrous oxide. *Front. Microbiol.* **3**, 61.

Grozeva N. G., Klein F., Seewald J. S. and Sylva S. P. (2017) Experimental study of carbonate formation in oceanic peridotite. *Geochim. Cosmochim. Acta* **199**, 264–286.

Helgeson H. C., Delany J. M., Nesbitt H. W. and Bird D. K. (1978) Summary and critique of the thermodynamic properties of rock-forming minerals. *Am. J. Sci.* **278A**, 1–229.

Hoehler, T. M., Borowski, W. S., Alperin, M. J., Rodriguez, N. M. and Paull, C. K. (2000). Model, stable isotope, and radiotracer characterization of anaerobic methane oxidation in gas hydrate-bearing sediments of the Blake Ridge. In Proceedings of the Ocean Drilling Program, Scientific Results (Vol. 164, pp. 79–85). Ocean Drilling Program College Station, Texas.

Hulme, S. M., Wheat C. G., Mottl M. J., and Fryer P. (2010). Porewater chemistry of the marina serpentinite mud volcanoes: a window to the seismogenic zone, Geochem. Geophys. Geosyst. 11, Q01X09, doi: 10.1029/2009GC002674.

Johnson J. W., Oelkers E. H. and Helgeson H. C. (1992) SUPCRT92: a software package for calculating the standard molal thermodynamic properties of minerals, gases, aqueous species, and reactions from 1 to 5000 bar and 0 to 1000 C. *Comput. Geosci.* **18**(7), 899–947.

Kawagucci S., Miyazaki J., Morono Y., Seewald J. S., Wheat C. G. and Takai K. (2018) Cool, alkaline serpentinite formation fluid regime with scarce microbial habitability and possible abiotic synthesis beneath the South Chamorro Seamount. *Prog. Earth Planet. Sci.* **5**(1), 74.

Kelley D. S., Karson J. A., Früh-Green G. L., Yoerger D. R., Shank T. M., Butterfield D. A., Hayes J. M., Schrenk M. O., Olson E. J., Proskurowski G. and Jakuba M. (2005) A

serpentinite-hosted ecosystem: the Lost City hydrothermal field. *Science* **307**(5714), 1428–1434.

Klein F. and McCollom T. M. (2013) From serpentinization to carbonation: new insights from a CO_2 injection experiment. *Earth Planet. Sci. Lett.* **379**, 137–145.

Klein F., Bach W., Jöns N., McCollom T., Moskowitz B. and Berquó T. (2009) Iron partitioning and hydrogen generation during serpentinization of abyssal peridotites from 15 N on the Mid-Atlantic Ridge. *Geochim. Cosmochim. Acta* **73**(22), 6868–6893.

Klein F., Bach W. and McCollom T. M. (2013) Compositional controls on hydrogen generation during serpentinization of ultramafic rocks. *Lithos* **178**, 55–69.

Klein F., Grozeva N. G., Seewald J. S., McCollom T. M., Humphris S. E., Moskowitz B., Berquó T. S. and Kahl W. A. (2015) Experimental constraints on fluid-rock reactions during incipient serpentinization of harzburgite. *Am. Mineral.* **100**(4), 991–1002.

Komor, S.C. and Mottl, M.J. (2005). Data Report: Stable isotope compositions of dissolved inorganic carbon, methane, sulfate and sulphide in pore water from the South Chamorro serpentinite mud volcano, Mariana subduction complex. In Proc. Ocean Drilling Program, Scientific Results.

Kyuno, A., Shintaku, M., Fujita, Y., Matsumoto, H., Utsumi, M., Watanabe, H., Fujiwara, Y. and Miyazaki, J.I. (2009). Dispersal and differentiation of deep-sea mussels of the genus Bathymodiolus (Mytilidae, Bathymodiolinae). Journal of Marine Biology.

Lancelot, Y., Larson, R., et al. (1990). Proc. ODP, Init. Repts. 129. College Station, TX (Ocean Drilling Program).

Latouche, C., Maillet N. and Blanchet R. (1981). X-ray mineralogy studies, Deep Sea Drilling Project Leg 60. In Init. Repts DSDP, 60 (eds. D.M. Hussong and S. Uyeda, et al.) U.S. Govt. Printing Office Washington, D.C., 437–454.

Maekawa, H., Shozui, M., Ishii, T., Saboda, K. and Ogawa, Y. (1992). 25. Metamorphic rocks from the serpentinite seamounts in the Mariana and Izu-Ogasawara forearcs. In P. Fryer, J. A. Pearce, Stokking, et al., Proceedings of the Ocean Drilling Program, Scientific Results (eds. P. Fryer, J. A. Pearce, Stokking, et al.) 125, 415–430.

Maekawa H., Shozul M., Ishll T., Fryer P. and Pearce J. A. (1993) Blueschist metamorphism in an active subduction zone. *Nature* **364**(6437), 520.

Maekawa H., Fryer P. and Ozaki A. (1995) Incipient blueschist-facies metamorphism in the active subduction zone beneath the Mariana forearc. *Active Margins and Marginal Basins of the Western Pacific Geophys. Monogr. Ser* **88**, 281–289.

McCollom T. M. (2016) Abiotic methane formation during experimental serpentinization of olivine. *Proc. Natl. Acad. Sci.* **113**(49), 13965–13970.

McCollom T. M. and Seewald J. S. (2006) Carbon isotope composition of organic compounds produced by abiotic synthesis under hydrothermal conditions. *Earth Planet. Sci. Lett.* **243**(1), 74–84.

McCollom T. M. and Bach W. (2009) Thermodynamic constraints on hydrogen generation during serpentinization of ultramafic rocks. *Geochim. Cosmochim. Acta* **73**(3), 856–875.

McCollom T. M., Klein F., Robbins M., Moskowitz B., Berquó T. S., Jöns N., Bach W. and Templeton A. (2016) Temperature trends for reaction rates, hydrogen generation, and partitioning of iron during experimental serpentinization of olivine. *Geochim. Cosmochim. Acta* **181**, 175–200.

McNichol J., Sylva S. P., Thomas F., Taylor C. D., Sievert S. M. and Seewald J. S. (2016) Assessing microbial processes in deep-sea hydrothermal systems by incubation at in situ temperature and pressure. *Deep Sea Res. Part I* **115**, 221–232.

Miyazaki J., Makabe A., Matsui Y., Ebina N., Tsutsumi S., Ishibashi J., Chen C., Kaneko S., Takai K. and Kawagucci S. (2017) WHATS-3: an improved flow-through multi-bottle fluid sampler for deep-sea geofluid research. *Front. Earth Sci.* **5**, 45. https://doi.org/10.3389/feart.2017.00045.

Mottl M. J. (2009) Highest pH. *Geochem News* **141**(09).

Mottl M. J., Komor S. C., Fryer P. and Moyer C. L. (2003) Deep-slab fluids fuel extremophilic Archaea on a Mariana forearc serpentinite mud volcano: Ocean Drilling Program Leg 195. *Geochem. Geophys. Geosyst.* **4**(11), 9009. https://doi.org/10.1029/2003GC000588.

Mottl M. J., Wheat C. G., Fryer, P., Gharib, J., Martin, J. B. (2004). Chemistry of springs across the Mariana forearc shows progressive devolatilization of the subducting slab. Geochim. Cosmochim. Acta 68, 4915–4933.

Oakley A. J., Taylor B., Fryer P., Moore G. F., Goodliffe A. M. and Morgan J. K. (2007) Emplacement, growth, and gravitational deformation of serpentinite seamounts on the Mariana forearc. *Geophys. J. Int.* **170**(2), 615–634.

Oakley A. J., Taylor B. and Moore G. F. (2008) Pacific Plate subduction beneath the central Mariana and Izu-Bonin fore arcs: new insights from an old margin. *Geochem. Geophys. Geosyst.* **9**(6).

Palandri J. L. and Reed M. H. (2004) Geochemical models of metasomatism in ultramafic systems: serpentinization, rodingitization, and sea floor carbonate chimney precipitation 1. *Geochim. Cosmochim. Acta* **68**(5), 1115–1133.

Phipps, S. and Ballotti, D. (1992). Rheology of Serpentinite Muds in the Mariana-Izu-Bonin Forearc. In: Proceedings of the Ocean Drilling Program, Scientific Results, 125, 363–372.

Pohlman J. W., Ruppel C., Hutchinson D. R., Downer R. and Coffin R. B. (2008) Assessing sulfate reduction and methane cycling in a high salinity pore water system in the northern Gulf of Mexico. *Mar. Pet. Geol.* **25**(9), 942–951.

Pons M. L., Quitté G., Fujii T., Rosing M. T., Reynard B., Moynier F., Douchet C. and Albarède F. (2011) Early Archean serpentine mud volcanoes at Isua, Greenland, as a niche for early life. *Proc. Natl. Acad. Sci.* **108**(43), 17639–17643.

Saffer D. M. and Tobin H. J. (2011) Hydrogeology and mechanics of subduction zone forearcs: fluid flow and pore pressure. *Annu. Rev. Earth Planet. Sci.* **39**, 157–186.

Salisbury, M. H., Shinohara, M., Richter, C., et al. (2002). Proc. ODP, Init. Repts., 195. College Station, TX (Ocean Drilling Program). doi:10.2973/odp.proc.ir.195.2002.

Saegusa S., Tsunogai U., Nakagawa F. and Kaneko S. (2006) Development of a multibottle gas-tight fluid sampler WHATS II for Japanese submersibles/ROVs. *Geofluids* **6**(3), 234–240.

Schoell M. (1980) The hydrogen and carbon isotopic composition of methane from natural gases of various origins. *Geochim. Cosmochim. Acta* **44**(5), 649–661.

Seyfried, Jr, W. E., Foustoukos D. I. and Fu Q. (2007) Redox evolution and mass transfer during serpentinization: an experimental and theoretical study at 200 C, 500 bar with implications for ultramafic-hosted hydrothermal systems at Mid-Ocean Ridges. *Geochim. Cosmochim. Acta* **71**(15), 3872–3886.

Seewald J. S., Doherty K. W., Hammar T. R. and Liberatore S. P. (2002) A new gas-tight isobaric sampler for hydrothermal fluids. *Deep Sea Res. Part I* **49**(1), 189–196.

Shock E. L. and Helgeson H. C. (1988) Calculation of the thermodynamic and transport properties of aqueous species at high pressures and temperatures: Correlation algorithms for ionic species and equation of state predictions to 5 kb and 1000 C. *Geochim. Cosmochim. Acta* **52**(8), 2009–2036.

Shock E. L., Helgeson H. C. and Sverjensky D. A. (1989) Calculation of the thermodynamic and transport properties of aqueous species at high pressures and temperatures: Standard

partial molal properties of inorganic neutral species. *Geochim. Cosmochim. Acta* **53**(9), 2157–2183.

Shock E. L., Sassani D. C., Willis M. and Sverjensky D. A. (1997) Inorganic species in geologic fluids: correlations among standard molal thermodynamic properties of aqueous ions and hydroxide complexes. *Geochim. Cosmochim. Acta* **61**(5), 907–950.

Soetaert K., Hofmann A. F., Middelburg J. J., Meysman F. J. R. and Greenwood J. (2007) The effect of biogeochemical processes on pH. *Mar. Chem.* **106**(1–2), 380–401.

Sverjensky D. A., Shock E. L. and Helgeson H. C. (1997) Prediction of the thermodynamic properties of aqueous metal complexes to 1000 C and 5 kb. *Geochim. Cosmochim. Acta* **61**(7), 1359–1412.

Takai K., Moser D. P., Onstott T. C., Spoelstra N., Pfiffner S. M., Dohnalkova A. and Fredrickson J. K. (2001) Alkaliphilus transvaalensis gen. nov., sp. nov., an extremely alkaliphilic bacterium isolated from a deep South African gold mine. *Int. J. Syst. Evol. Microbiol.* **51**(4), 1245–1256.

Takai K., Moyer C. L., Miyazaki M., Nogi Y., Hirayama H., Nealson K. H. and Horikoshi K. (2005) Marinobacter alkaliphilus sp. nov., a novel alkaliphilic bacterium isolated form subseafloor alkaline serpentinite mud from Ocean Drilling Program Site 1200 at South Chamorro Seamount, Mariana forearc. *Extremophiles* **9**, 17–27. https://doi.org/10.1007/s00792-004-0416-12005.

Vinas, Keri A., Mariana Forearc Crust CORK Pressure Data: Observations and Implications (2013). Open Access Theses. Paper 436.

Wheat C. G. and McDuff R. E. (1994) Hydrothermal flow through the Mariana Mounds: Dissolution of amorphous silica and degradation of organic matter on a mid-ocean ridge flank. *Geochim. Cosmochim. Acta* **58**(11), 2461–2475.

Wheat C. G. and Mottl M. J. (1994) Hydrothermal circulation, Juan de Fuca Ridge eastern flank: factors controlling basement water composition. *J. Geophys. Res. Solid Earth* **99**(B2), 3067–3080.

Wheat C. G. and Fisher A. T. (2008) Massive, low-temperature hydrothermal flow from a basaltic outcrop on 23 Ma seafloor of the Cocos Plate: chemical constraints and implications. *Geochem. Geophys. Geosyst.* **9**(12).

Wheat C. G., Fryer P., Fisher A. T., Hulme S., Jannasch H., Mottl M. J. and Becker K. (2008) Borehole observations of fluid flow from South Chamorro Seamount, an active serpentinite mud volcano in the Mariana forearc. *Earth Planet. Sci. Lett.* **267**(3–4), 401–409.

Wheat, C.G., Fournier, T., Paul, C., Menzies, C., Price, R.E., Ryan, J. and Sissman, O., Data report: IODP Expedition 366 pore water trace element (V, Mo, Rb, Cs, U, Ba, and Li) compositions. In Fryer, P., Wheat, C.G., Williams, T., and the Expedition 336 Scientists Proceedings of the International Ocean Discovery Program, Volume 366, 366, 2018, 1-8.

Whiticar M. J. (1999) Carbon and hydrogen isotope systematics of bacterial formation and oxidation of methane. *Chem. Geol.* **161**(1–3), 291–314.

Wolery, T.J., 1992. EQ3/6, a software package for geochemical modeling of aqueous systems: package overview and installation guide (version 7.0).

Yoshinaga M. Y., Holler T., Goldhammer T., Wegener G., Pohlman J. W., Brunner B., Kuypers M. M., Hinrichs K. U. and Elvert M. (2014) Carbon isotope equilibration during sulphate-limited anaerobic oxidation of methane. *Nat. Geosci.* **7**(3), 190.

Associate editor: Wolfgang Bach